Impact Properties and Microhardness of Double-Gated Glass-Reinforced Polypropylene Injection Moldings

Matias Martinez Gamba,[1] António Sergio Pouzada,[2] Patricia María Frontini[1]
[1] *Instituto de Investigaciones en Ciencia y Tecnología de Materiales (INTEMA), Universidad Nacional de Mar del Plata, Av. Juan B. Justo 4302, B7608FDQ, Mar del Plata, Argentina*

[2] *IPC/Institute for Polymers and Composites, University of Minho, 4800-058 Guimarães, Portugal*

Injection moldings with weld lines were produced in glass reinforced polypropylene grades differing in filler content using a two-gated hot runner injection mold. The skin-core microstructure developed during injection molding was qualitatively analyzed by means of optical and scanning electronic microscopy techniques. The load bearing capacity of the moldings was assessed by uniaxial tensile-impact and biaxial instrumented falling dart impact tests. Microhardness was also used to ascertain the possibility of using it as a simple nondestructive technique for characterizing glass fiber-reinforced injection moldings. The properties were monitored at various points to evaluate their variation at the bulk and the knit region. The biaxial impact test highlights the 10-fold reduction of the impact strength caused by the weld line. POLYM. ENG. SCI., 00:000–000, 2009. © 2009 Society of Plastics Engineers

INTRODUCTION

Polymeric injection moldings are currently used in many application areas, namely in the automotive sector. The increasing use of polymers is greatly associated to cost reduction resulting from lower weight, elimination of secondary operations, and use of less energy. Nonetheless, the influence of processing parameters is critical in the performance of these products. Hot runner molds are adequate to mass production as in the automotive industry. These molds lead to the reduction of production costs by saving material of the nonrequired gating system and by shortening the cycle time. Furthermore, lower injection pressure is required, the process temperature is controllable with greater precision, more uniform filling is achievable in multicavity molds, and thus, the final mechanical properties of the moldings are improved [1].

Correspondence to: Patricia Frontini; e-mail: pmfronti@fi.mdp.edu.ar
Contract grant sponsor: EU ALFA project Plastinet-master (Department of Polymer Engineering, University of Minho).
DOI 10.1002/pen.21393
Published online in Wiley InterScience (www.interscience.wiley.com).

Polypropylene (PP) is a material that is used widely in many applications because of its very attractive cost/performance ratio [2]. Glass-reinforced PP grades are current alternatives to more expensive engineering materials for structural parts. The improved mechanical properties, good dimensional stability, very low moisture absorption, and high creep resistance, even at high temperatures are in favor of the use of glass-reinforced grades. Typical applications include, for example, electrical components, load bearing automotive parts, interior, exterior, and under the bonnet, force transmission parts or structural furniture parts. Features related to mechanical properties of PP-glass fiber composites have been described in the literature: the variation of elastic modulus with the amount and orientation of reinforcement [3], the reduction of impact strength with increasing processing temperature [4], and the influence of fiber length and concentration on impact strength [5]. The influence of injection molding conditions and glass fiber contents on the mechanical behavior of injection molding glass fiber polypropylene composites was thoroughly assessed by Ota et al. [6].

The fiber direction and distribution in the moldings influence the mechanical strength of the composites. The fiber orientation field is established during the flow of the polymer in the mold. The melt flow inside the impression is a complex thermo-mechanical process with characteristics changing from point to point within the whole volume of the part. When the flow develops with high shear stresses the fibers tend to align in the flow direction, whereas a predominantly extensional flow tends to align the fibers in the principal extension direction. The resulting morphology is complex and is related to those alignment effects and to the variation of the cooling rate throughout the part. Finally, the flow-induced fiber orientation field causes the molded part to show anisotropic properties that are essential in its mechanical performance [7–9].

The presence of weld lines in injection moldings is a major design concern. The weld lines can lead to a considerable reduction in the mechanical properties and so

designers often need to use larger safety factors in the design analysis to compensate for that weakness. Weld lines are almost impossible to avoid in injection molding, especially when multiple gating or inserts are used, or holes exist in the molding. The position and strength of a weld line affect the injection molding performance, especially when the part is subjected to mechanical loading. Mielewski et al. [10] who studied the formation of weld lines in unfilled PP showed that the depth of the V-notch generated at the molding surface is related to the injection temperature, mold temperature, and injection speed. They also assessed the effect of pores and cavities that occur in the bulk of the part as a result from three melt fronts meeting together and impeding the entrapped air from escaping the mold. When discontinuous glass fibers are used as reinforcement, these problems are worsened by the inherent anisotropy of the polymer composite. The reduction in mechanical strength and fracture toughness of injection-molded glass fiber-reinforced moldings with weld lines has been reported by several authors who analyzed cold and hot weld lines in moldings of different geometries [11–14]. Generally, the reduction of strength at the weld line decreases with the increasing fiber content and is related to unfavorable molecular or fiber orientation at the knit region [15]. More specifically, Fisa and Rahmani [16] studied the strength of weld lines formed around an obstacle in injection molded fiber-reinforced PP and stated that the weld line strength is a function of the fiber content only.

As an alternative to usual mechanical characterization methods, Boyanova et al. [17] argued that microhardness can be used, as a nondestructive technique, to characterize fiber-reinforced composites and provide information on their heterogeneity. Microhardness has been successfully used to provide information about the dependence of properties on the processing parameters near to and at the weld line, and also about the correlation between other mechanical properties and the microstructure [18, 19].

The motivation of this work was to explore the possibility of correlating microhardness with mechanical properties of glass-reinforced PP injection moldings, as suggested by Baltá-Calleja and coworkers for similar polymeric systems [19–21]. Hence, grades of glass fiber-reinforced PP were injected using a two-gate hot runner mold in which a weld line is generated by the two incoming flow fronts. Standard tensile-impact and instrumented falling weight testing were chosen as the macromechanical characterizing technique for assessing the performance of the moldings. Microhardness and impact measurements were done at various radial positions from the gate to the weld line.

EXPERIMENTAL

Materials

The materials used in this study are commercial short glass fiber-reinforced PP injection molding grades PP G2 N01, PP G3 N01, and PP G4 R01 (Hostacom from Basell, Tarragona, Spain) with nominal glass fiber contents of 20, 30, and 40%, respectively. Their glass fiber content (GF), density (δ), melt flow rate (MFR according to ISO 1133, 2.16 kg/230°C), melting temperature (T_m), and PP crystallinity (X_c, determined by DSC) are shown in Table 1.

TABLE 1. Material properties.

Material	GF (%)	δ (Mg/m^3)	MFR (g/600 s)	T_m (°C)	PP X_c (%)
PP20%GF	20.7	1.04	1.68	167.6	46.8
PP30%GF	30.6	1.13	1.35	167.7	44.3
PP40%GF	40.3	1.22	3.00	167.7	38.4

The overall crystalline fraction (X_c) was calculated as:

$$X_c = \frac{\Delta H_f}{\Delta H_{f,c}} \quad (1)$$

where ΔH_f is the experimental heat of fusion, and $\Delta H_{f,c}$ is the heat of fusion of a pure crystalline PP, which was taken as 207.1 J/g [22, 23].

Throughout the paper, these three materials will be referred to as PP20%GF and PP30%GF, PP40%GF, according to the filler content.

In spite of the manufacturer not disclosing information on the raw material of the matrix, it clearly appears from the data on Table 1 that the characteristics of the PP matrix of the PP40%GF composite is definitely different from the others. Judging from the lower crystallinity and the MFR of this composite, it can be concluded that the PP matrix is different from the others and has a definitely lower molecular weight. This manufacturer's option for the 40% filled composite was probably devised to improve processing at such high filler content.

Injection Molding

Mold and Molding. The materials were injected in a mold with a hot runner system feeding in two points, an impression for molding a rectangular box with dimensions of 73 × 152 × 16 (mm) and wall thickness of 1.4 mm, as shown in Fig. 1. The two injection gates are 67 mm apart and originate a weld line starting at the center of the molding.

Injection Molding. The moldings were produced using a Klöckner Ferromatic Desma FM20 injection molding machine of 200 kN clamping force. The processing conditions were adjusted to each of the materials considered in the study, namely, injection temperatures: 250°C and 280°C; injection time: 1 s; mold temperature: 50°C; holding pressure: 3 MPa.

Test Samples

The test pieces for subsequent mechanical characterization were obtained by machining from the moldings

 DOI 10.1002/pen

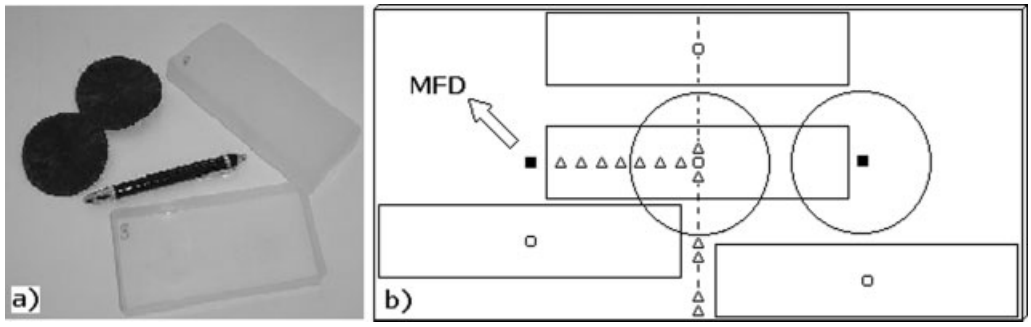

FIG. 1. (a) Double-gated injected parts. (b) Scheme of the molding showing the location of impact test specimens (rectangular samples for tensile impact and discs for falling weight impact); weld line (–); injection points (■) and microhardness test points (△). Arrow indicates melt flow direction (MFD).

according to standard geometries. Rectangular specimens of 10 mm width and a hole of 3 mm diameter at the center were used for the tensile-impact tests. The falling weight impact tests were carried out on 55 mm in diameter circular discs. The variation in toughness at the weld and the bulk regions was obtained from samples taken at locations according to the layout in Fig. 1.

Sample Testing

Microscopy. The trough-thickness fiber orientation induced during the filling of the moldings was observed using the technique of reflective light microscopy using an Olympus BH2 setup on surface polished samples. The images were assessed with a digital acquisition Leica Quantimet 500+ image analyzer.

Scanning electronic microscopy using JEOL JSM-6460 LV equipment was applied for the observation of fractured surfaces that were previously coated with Au-Pd.

Microhardness. Microhardness measurements were performed using the microhardness tester Leica WMHT 30A, adapted with a Vickers square-based diamond indenter. The hardness was calculated from the diagonal of the residual indentation according to the *Eq. 2* [24].

$$\mathrm{HV} = \frac{2 \times P \times \sin\left(\frac{\alpha}{2}\right)}{d^2} = \frac{1,854 \times P}{d^2} \qquad (2)$$

To minimize the effect of the secondary phase and creep, a load of 20 N and indentation time of 5 s were used. Measurements were taken at the locations shown in Fig. 1.

Tensile-Impact Strength. The effect of the weld line on the mechanical properties of a given polymer is usually estimated by testing in impact mode tensile specimens molded with and without a weld line. The specimens in this study were tested with a standard pendulum Ceast 6545 at room temperature fitted with ancillaries for tensile-impact testing. The impact velocity was of 3.6 m/s according to the ISO 8256 standard. The impact strength is calculated as the energy to break the specimen divided by the resisting cross sectional area.

Instrumented Falling Weight Impact. The impact tests with loading perpendicular to the plane containing one of the injection points (IP) were carried according to the ASTM D 5628-94 standard using the Ceast FRACTOVIS equipment. This equipment allows the load on the specimen to be continuously recorded as a function of time prior to fracture. This gives a much more complete representation of an impact than a single calculated value. The specimens were clamped between two steel plates with a circular opening of 40 mm in diameter. A velocity at impact of 3 m/s was used. This technique is widely accepted for the out-of-plane fracture response assessment of polymeric composites because it gives a realistic view of in-service impact situations, hence being closer to real life conditions [25–27]. From the energy vs. displacement plots, the thickness-related maximum load F_{max}/t and the thickness-related perforation energy E_{per}/z were computed [28].

RESULTS AND DISCUSSION

Fiber Orientation

During the injection molding processes, complex flow patterns resulting from the complex interaction between melt properties, mold geometry, and molding conditions are likely to happen in the impression. When the cooling rate is fast, a very heterogeneous fiber orientation field builds up. This orientation field causes the molded part to acquire anisotropic properties. Thus, the knowledge of the relationship between processing, structure, and property of injection molded short fiber composites is essential to predict their mechanical performance. Because of the initial radial flow direction (MFD in Fig. 1), the fibers adopt a radial organization close to the injection points, as illustrated in the SEM picture shown in Fig. 2.

As the melt spreads radially in the impression, a divergent flow develops, orienting fibers and polymer molecu-

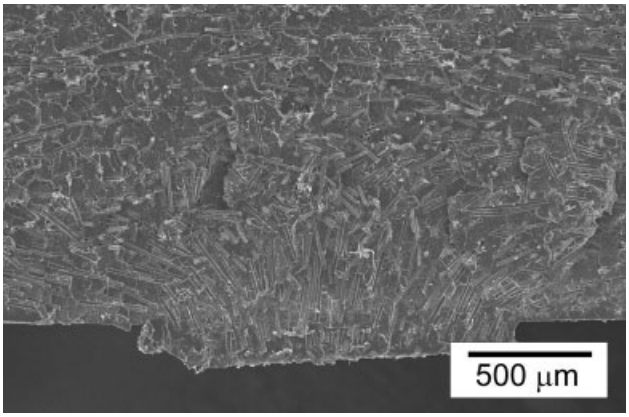

FIG. 2. SEM view of a fractured surface of a PP20%GF molding near to an injection point.

lar chains with a complex pattern resulting from the effect of the shear and the elongation flows (e.g., [7, 8]): at the core the fibers are transversely oriented by in-plane stretching; at the skins the fibers become aligned by the high shear stresses close to the surfaces. Figure 3 shows optical micrographs of polished cross sections of a molded sample with 30% glass fibers taken at different locations. Away from the weld zone a skin-core structure developed according to the local flow pattern and mold geometry (Fig. 3a and b). Here, shear flow dominates and produces fairly uniform levels of fiber alignment perpendicular to the main flow direction. The skin-core structure was practically not visible in the section containing the knit line where fibers appear mainly oriented parallel to the weld plane (Fig. 3c).

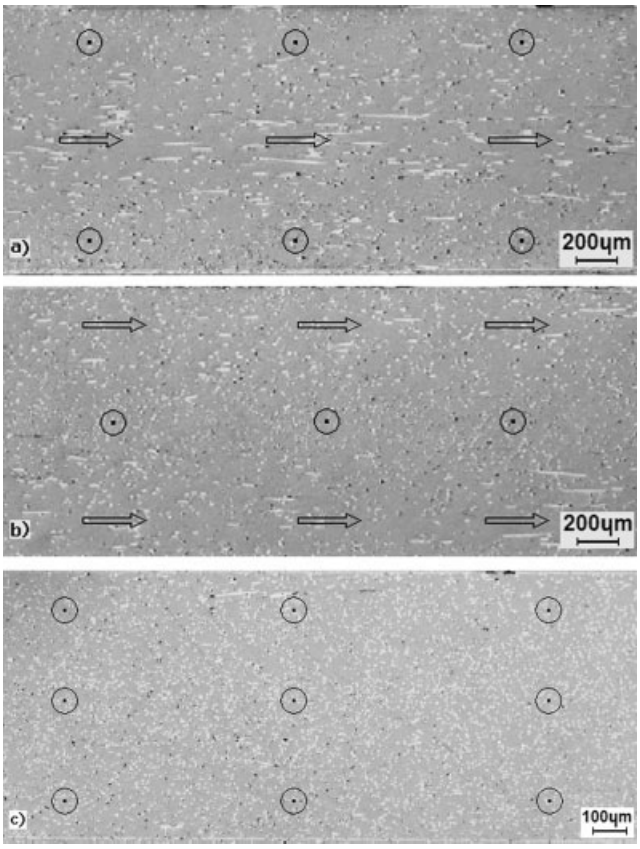

FIG. 3. Cross-sectional optical micrograph of a PP30%GF molding. The arrows correspond to regions where fibers align in that direction. The circles with a dot indicate areas where the fibers orient preferably perpendicular to the picture plane. (a) Fiber orientation in the bulk zone: observation plane is parallel to weld line plane. (b) Fiber orientation in the bulk zone: observation plane is orthogonal to weld line plane. (c) Fiber orientation in the weld line: observation plane is orthogonal to weld line plane.

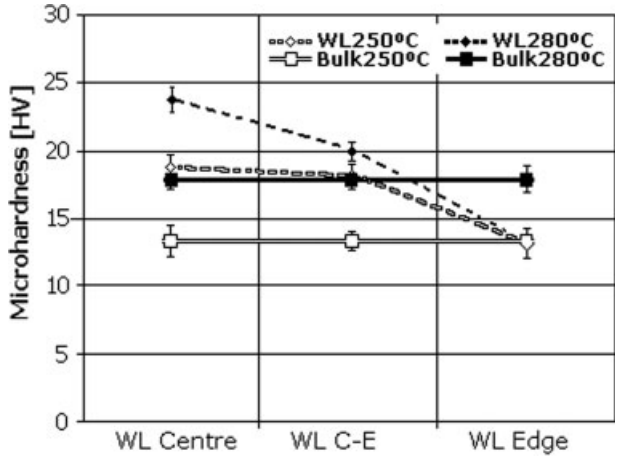

FIG. 4. Microhardness variation along the weld line. Material: PP30%GF.

This varying orientation of the fibers confirms the significant influence of the geometry of the mold. Important features are the location of the gates and the flow path length.

Microhardness

Effect of the Processing Conditions. The effect of processing conditions on the microhardness is illustrated

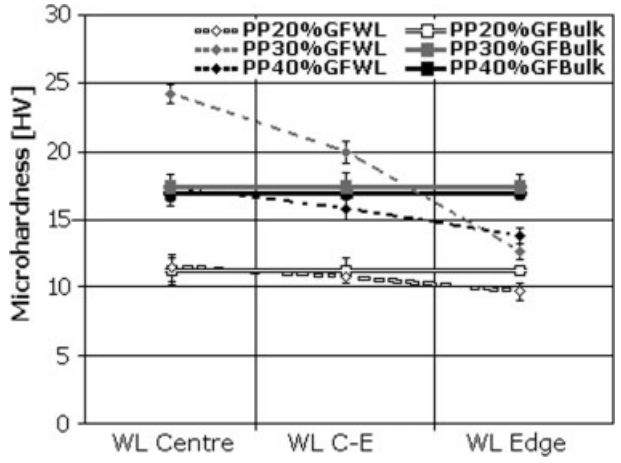

FIG. 5. Effect of the fiber content in the microhardness at bulk and WL.

DOI 10.1002/pen

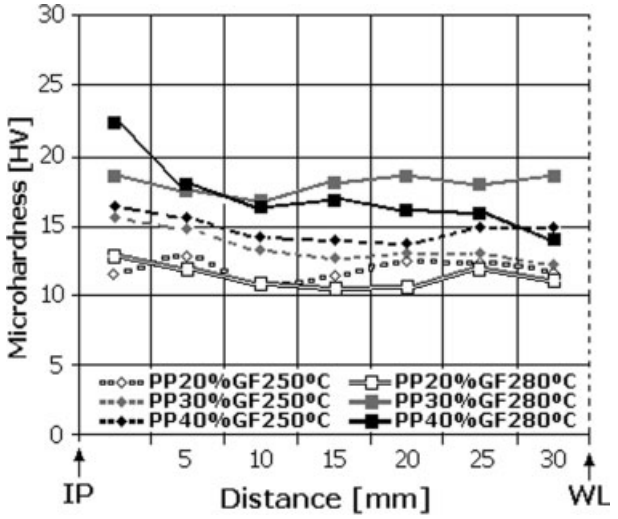

FIG. 6. Variation of the microhardness from the injection point, IP, to the weld line location, WL.

for PP30%GF in Fig. 4, as an example. There is a slight microhardness increase in parts molded at higher temperature. The difference is more evident in the weld area at the center of the molding, but drops towards the edges of the piece. This suggests that the microstructure developing at the weld line location is different, as it is unlikely that the microhardness is affected by the presence of the fibers.

Effect of the Fiber Content. Figure 5 includes test data, obtained at the bulk and weld line regions, for the two injection temperatures (250°C and 280°C). It is observable again that the microhardness at the weld line region drops towards the edges of the molding. This effect is more pronounced with PP30%GF, where there is

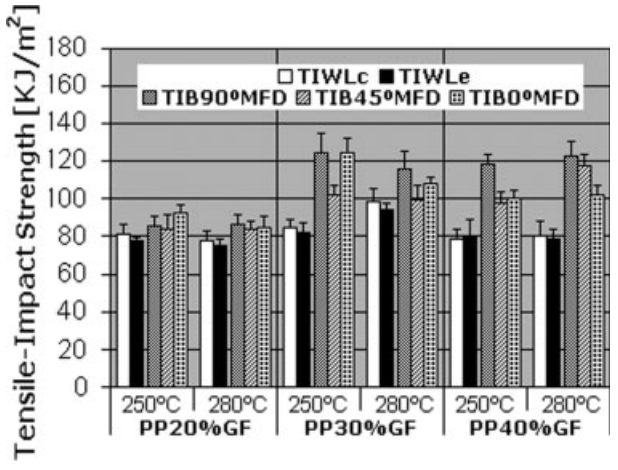

FIG. 7. Tensile impact strength of various PP glass reinforced moldings. TIB90°MFD: values taken at bulk at 90° of the melt flow direction. TIB45°MFD: values taken at bulk at 45° of the melt flow direction.- TIB0°MFD: values taken at bulk at 0° of the melt flow direction. TIB WLc: values taken at the central point of the weld line. TIB WLe: values taken at the extreme points of the weld line.

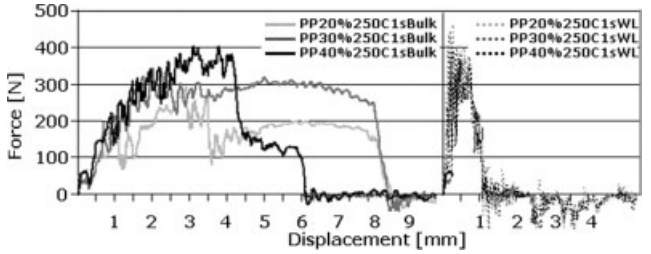

FIG. 8. Fracture Surface of PP30%GF at weld line showing scarce fiber pull-out in agreement with the low energy achieved.

a clear increase at the central areas of the WL region. This different behavior is attributable to the combined effect of fiber content and PP matrix characteristics that lead to the highest overall MFI (see Table 1).

As shown in Fig. 6, there are no sizeable variations in the microhardness at the bulk as the test point moves away from the injection point. Nevertheless and in spite of some data dispersion, close to the injection point, the microhardness is slightly higher.

Impact

Tensile-Impact Strength. The variation of tensile-impact strength at the selected testing location points, at various injection temperatures is shown in Fig. 7.

The impact strength of PP20%GF moldings does not vary significantly with the test location and processing conditions (81 ± 5 kJ/m^2). On the contrary, much higher and scattered data were yield by the other two grades: PP30%GF is generally stronger with 88 ± 10 kJ/m^2 at WL and 113 ± 13 kJ/m^2 at the bulk; the impact strength of PP40%GF is slightly lower and not improving with the processing temperature as occurs with the PP30%GF molded at 280°C. The test data at the bulk were practically not affected by the processing conditions as reported before by Koster [29]. The weld line impact strength at the weld lines was always at least 70% of the bulk, and decreased as the fiber content increased.

The reduction in weld line impact strength is caused by the fibers at weld line assuming an orientation which

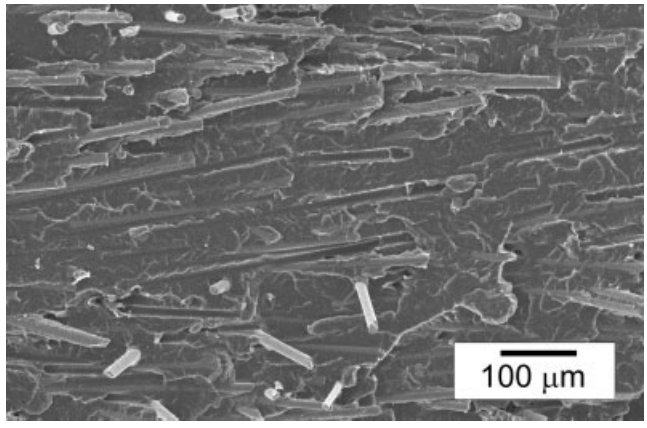

FIG. 9. Falling weight impact tests, out of-plane toughness assessment.

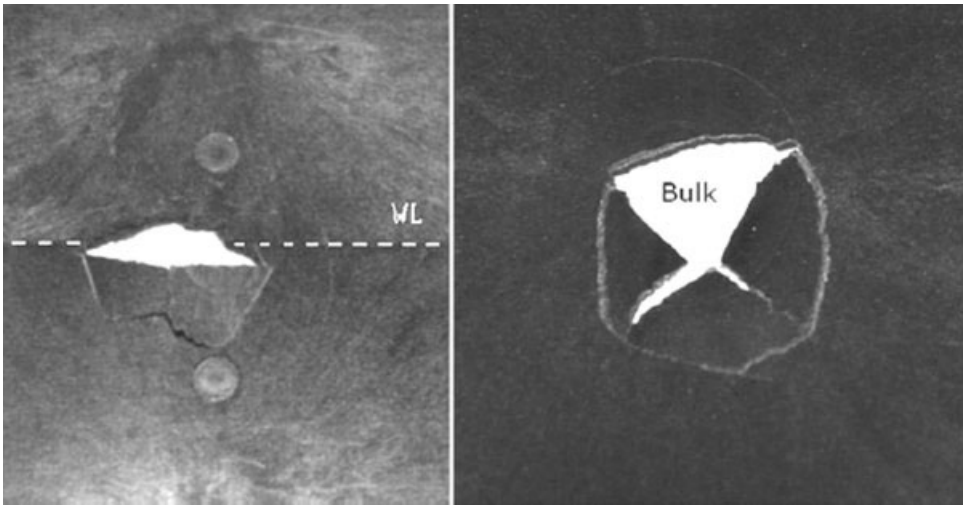

FIG. 10. Falling weight impact tests, fracture pattern at weld line, and bulk zones.

is parallel to the weld line and perpendicular to the direction of the applied stress in the tensile-impact test, as explained before. It is well known that in transverse tensile loading the fibers act only as hard inclusions in the matrix instead of load-carrying members, and no pull-out is promoted [30].

Out-of-Plane Toughness. The recorded drop-weight dart impact test data and fracture surfaces and (force-displacement curve) as a function of the fiber content and impact location (i.e., bulk and WL) are depicted in Figs. 8–13.

The instrumented nature of this test allows also observing how the energy is absorbed and how the fracture process develops in each case. Specimens impacted at locations away from the WL initially displayed a monotonically increasing force-displacement trend. Beyond the maximum, the force discontinuously drops to zero during longer times. On the contrary, specimens impacted at the WL failed in a brittle manner immediately after the maximum force is reached and after a very small deflection. The biaxial impact performance data are summarized in Table 2.

Analyzing the data at bulk locations, the force peak and the total energy fracture increase with fiber content with a concomitant loss of ductility as judged from the final deflection of the samples. In fact, it is well known that any improvement in stiffness and strength comes at the cost of ductility.

The peak force was practically insensitive to the impact position and fiber content, but the total impact energy varied markedly between bulk and WL. Again, no significant differences were observed between samples processed with different conditions. The total perforation energy at the weld lines was one order of magnitude lower due to the much smaller deflection at total failure (Table 2).

The macroscopic analysis of the fractured surfaces shown in Fig. 10 provides additional insight of the differences in the mechanical behavior. This test does not impose a preferential direction of failure in the specimen.

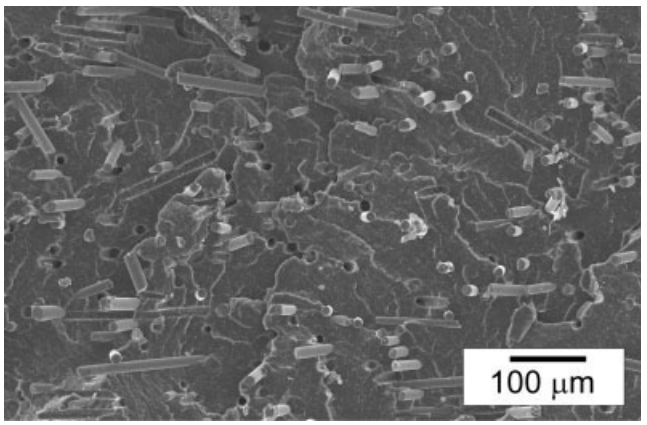

FIG. 11. Fracture surface of PP20%GF showing fiber pull out.

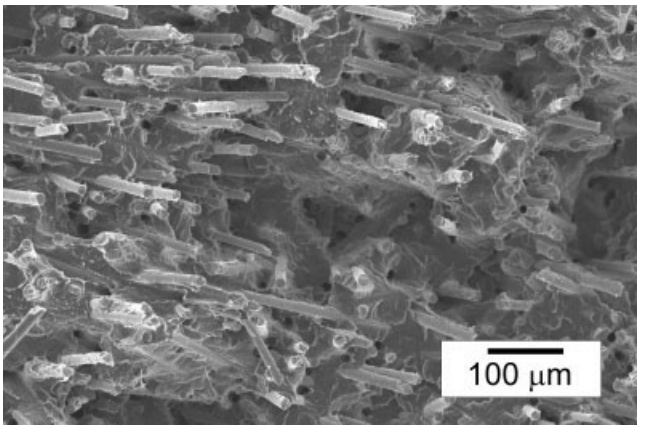

FIG. 12. Fracture surface of PP30%GF showing matrix drawing.

 DOI 10.1002/pen

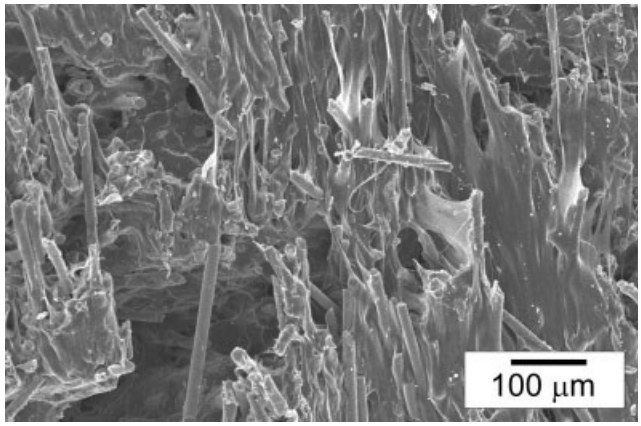

FIG. 13. Fracture surface of PP40%GF showing extensive matrix drawing.

Consistently, isotropic or orthotropic materials are expected to display a symmetric deformation pattern to the impact site. The failures originate at the weakest point in the sample and propagate from there due to the high radial and circumferential tensile stresses [31]. The two images in Fig. 10 suggest that the failures occur in a brittle manner but the fracture patterns are significantly different. The samples impacted at the bulk show that the fracture proceeded by cracks that run radially from the central point of impact. This is consistent with the fiber orientation at the skin layer being parallel to the melt flow direction, where the stresses resulting from impact are higher and consequently the failure process starts. The direction perpendicular to the fiber orientation corresponds to least resistance, thus several cracks develop radially in the direction of the fiber orientation. On the contrary, samples impacted at the weld lines display a fracture that runs along the weaker weld line direction.

Typical fracture surfaces of PP20%GF, PP30%GF, and PP40%GF samples impacted at bulk regions are shown in Figs. 11–13. Massive fiber pull-out is evident in the cases of PP20%GF and PP30%GF confirming that the fibers were not pretreated (coupled) before compounding with the PP.

The larger plastic deformation in the reinforced matrix observed in the PP40%GF samples (see Fig. 11) indicate a better adhesion between the fibers and the polymer in the matrix, which supposedly and as mentioned in the "Materials" section is different from that used in compounding the PP20%GF and PP30%GF grades.

When impact was performed on the weld lines, rare fiber pullout was observed and it is evident that the failure occurred predominantly perpendicular to the fiber direction (see Fig. 9). Also the energy required for causing failure is much lower than at the bulk.

Hardness to Impact Strength Correlation

The correlation between tensile-impact strength and microhardness was assessed by determining the linear correlation coefficients. The correlation is considered statically insignificant when the coefficient is less than 0.8. The coefficients for the three materials studied are shown in Table 3.

The very low correlation coefficients indicate that no clear correlation between the two variables exists. This lack of correlation confirms recent statements by Krumova et al. [32] that the microhardness analysis of composites seems to be not simple because the contribution of the fibers to the global hardness depends not only on the fiber content but also on their distribution. Also a simple rule of mixtures that is postulated for nonreinforced glassy and semi-crystalline polymers [19] cannot be assumed in this case because, in a microhardness test, the filler does not contribute its real hardness value to the measured hardness. The reason may be that the contribution to microhardness during the test from a vertical fiber differs from that from a horizontal one.

CONCLUSIONS

The mechanical performance of fiber reinforced-polypropylene injection moldings with weld lines was assessed in terms of the fiber content and processing conditions on microhardness and impact strength.

TABLE 2. Falling weight impact test data.

		Bulk			Weld line		
Material	t_i (s)	F_{max}/z (N/mm)	Displ. (mm)	E_{per}/z (J/mm)	F_{max}/z (N/mm)	Displ. (mm)	E_{per}/z (J/mm)
PP20%GF	0.5	225	2.89	389	229	0.53	30
	1	211	2.78	403	264	0.68	31
	1.5	208	2.63	414	209	0.44	33
PP30%GF	0.5	256	2.58	589	246	0.51	46
	1	248	2.34	604	292	0.58	50
	1.5	251	2.40	627	254	0.67	51
PP40%GF	0.5	264	3.48	389	282	0.44	31
	1	288	3.12	408	329	0.38	33
	1.5	278	3.39	414	299	0.52	34

TABLE 3. Correlation between tensile impact strength and microhardness.

	PP20%GF		PP30%GF		PP40%GF	
	Ti: 250°C	Ti: 280°C	Ti: 250°C	Ti: 280°C	Ti: 250°C	Ti: 280°C
Correlation coefficient R^2	0.307	0.097	0.002	0.171	0.001	0.198

The mechanical performance of the moldings was practically not affected by the processing conditions, which suggests that the matrix morphology may be not the leading factor in this type of materials.

Bulk microhardness was practically constant from center to edge with a slight increasing trend with fiber content. On the contrary, the microhardness along the weld lines decreases from the central point to the edges.

The uniaxial tensile-impact strength at weld lines locations displayed an average decay between 20 and 30% when compared with that of the bulk, whereas the biaxial falling weight impact test, which represents better in-service situations, decreased by 10-fold on average. The deciding factor for the decrease is the unfavorable fiber orientation in the weld line region.

The falling weight impact test appears to be very sensitive to fiber content and presence of weld lines. Biaxial loading imposes a more severe and realistic loading condition than uniaxial loading. In bending, the outer layer of the sample is more stressed than the core, whereas in tension the stress is uniformly distributed over the resisting area. There is no significant correlation between microhardness and impact strength probably due to the complex pattern of fiber distribution and complex relationship between microhardness and fiber content.

REFERENCES

1. A. Demirer, Y. Soydan, and A.O. Kapti, *Mater. Des.*, **28**, 1467 (2007).
2. R.A. Malloy, *Plastic Part Design for Injection Molding—An Introduction*, Hanser, Cincinnati (1994).
3. N.J. Lee and J.S. Jang, *Compos. Part A Appl. Sci.*, **30**, 815 (1999).
4. N.M. Neves, A.J. Pontes, J.C. Velosa, A.R. Faria, and A.S. Pouzada, *Key Eng. Mater.*, **230**, 52 (2002).
5. W.Y. Chiu, H.C. Lu, and C.L. Chang, *J. Appl. Polym. Sci.*, **43**, 1335 (1991).
6. W.N. Ota, S.C. Amico, and K.G. Satyanarayana, *Comp. Sci. Technol.*, **65**, 873 (2005).
7. N.M. Neves, A.J. Pontes, and A.S. Pouzada, *J. Reinf. Plast. Comp.*, **20**, 452 (2001).
8. J.S. Cintra, A.S. Pouzada, and J.A. Sousa, PPS-15 Polymer Processing Society Conference Proceedings, paper No. 331 (1999).
9. A. Gullu, A. Ozdemir, and E. Ozdemir, *Mater. Des.*, **27**, 316 (2006).
10. D.F. Mielewski, D.R. Bauer, P.J. Schmitz, and H. Van Oene, *Polym. Eng. Sci.*, **38**, 2020 (1998).
11. A. Chrysostomou and S. Hashemi, *J. Mater. Sci.*, **33**, 4491 (1998).
12. S. Patcharaphun, B. Zhang, and G. Mennig, *J. Reinf. Plast. Compos.*, **26**, 977 (2007).
13. Z.U. Nabi and S. Hashemi, *J. Mater. Sci.*, **33**, 2985 (1998).
14. S. Hashemi and M. Koohgilani, *Polym. Eng. Sci.*, **35**, 1124 (1995).
15. C.H. Wu and W.J. Liang, *Polym. Eng. Sci.*, **45**, 1021 (2005).
16. B. Fisa and M. Rahmani, *Polym. Eng. Sci.*, **31**, 1330 (1991).
17. M. Boyanova, F.J. Baltá-Calleja, S. Fakirov, I. Kuehnert, and G. Mennig, *Adv. Polym. Technol.*, **24**, 14 (2005).
18. M.C. García Gutiérrez, D.R. Rueda, F.J. Baltá-Calleja, I. Kuehnert, and G. Mennig, *J. Mater. Sci. Lett.*, **18**, 1237 (1999).
19. F.J. Baltá-Calleja and S. Fakirov, *Microhardness of Polymers*, Cambridge University Press, Cambridge (2000).
20. W.P. Paplham, J.C. Seferis, F.J. Baltá-Calleja, and H.G. Zachmann, *Polym. Compos.*, **16**, 424 (1995).
21. A. Flores, F.J. Baltá-Calleja, G.E. Attenburrow, and D.C. Bassett, *Polymer*, **41**, 5431 (2000).
22. H.S. Bu, S.Z.D. Cheng, and B. Wunderlich, *Makromol. Chem. Rapid. Commun.*, **9**, 75 (1988).
23. J. Brandrup, E.H. Immergut, and E.A. Grukle, Eds., *Polymer Handbook*, Wiley, New York (1999).
24. F.J. Baltá-Calleja, M.E. Cagiao, R. Adhikari, and G.H. Michler, *Polymer*, **45**, 247 (2004).
25. J. Karger-Kocsis, *Compos. Sci. Technol.*, **48**, 273 (1993).
26. A.M. Cunha and A.S. Pouzada, in *Impact and Dynamic Fracture of Polymers and Composites*, J.G. Williams and A. Pavan, Eds., Mechanical Engineering Publications, London (1995).
27. E.L. Rodriguez, *J. Mater. Sci.*, **25**, 5269 (1990).
28. J. Karger-Kocsis, E. Moos, I. Mudra, and J. Varga, *J. Macromol. Sci. Phys.*, **38**, 647 (1999).
29. R.P. Koster, *J. Inj. Mold. Technol.*, **3**, 154 (1999).
30. P.K. Mallick, *Fiber-Reinforced Composites-Materials, Manufacturing and Design*, *2nd ed.*, CRC Press, Boca Raton (1993).
31. B. Alcock, N.O. Cabrera, N.M. Barkoula, and T. Peijs, *Comp. Sci. Technol.*, **66**, 1724 (2006).
32. M. Krumova, C. Klingshirn, F. Haupert, and K. Friedrich, *Comp. Sci. Technol.*, **61**, 557 (2001).